Advances in Aerospace Science and Technology, 2022, 7, 97-111
https://www.scirp.org/journal/aast
ISSN Online: 2473-6724
ISSN Print: 2473-6708

Interference Detection and Suppression Based on Time-Frequency Analysis

Haijun Huang, Kewen Sun

Hefei University of Technology, Hefei, China
Email: 2019170896@mail.hfut.edu.cn

How to cite this paper: Huang, H.J. and Sun, K.W. (2022) Interference Detection and Suppression Based on Time-Frequency Analysis. *Advances in Aerospace Science and Technology*, **7**, 97-111.
https://doi.org/10.4236/aast.2022.72006

Received: March 17, 2022
Accepted: May 15, 2022
Published: May 18, 2022

Abstract

Radio frequency interference (RFI) is greatly harmful to Global Navigation Satellite System (GNSS) receivers. Sweep interference is one of the RFI for the GNSS receivers, which can degrade the performance of GNSS receivers seriously. In this paper, the Fractional Fourier Transform (FrFT) of time-frequency analysis is proposed in the GNSS interference detection and suppression. The FrFT method is tested for detecting and suppressing sweep interference, which is generated by a GNSS jammer. In the simulation experiment, the GNSS signal affected by sweep frequency interference is successfully captured after interference suppression by using the proposed method, which shows its effectiveness. The interference detection performance of the FrFT method is compared with the conventional techniques such as Short-Time Fourier transform (STFT) and Wigner-Ville distribution (WVD). The detection performance is improved by about a least one order of magnitude. In the aspect of interference suppression, a threshold method based on detection probability is proposed, and the performance of the proposed threshold method is compared with the conventional threshold methods. In the result, the interference tolerance is increased by 5 dB compared with the mean threshold method, and by 9 dB compared with the fixed threshold.

Keywords

RFI, GNSS, Sweep Interference, FrFT, STFT, WVD, Threshold

1. Introduction

At present, the GNSS) has been widely used in many fields, and its effectiveness has been recognized by the world [1] [2]. The GNSS receiver is extremely vulnerable to natural and man-made electromagnetic interference [3] [4]. Satellite navigation systems are facing the challenge of ensuring high accuracy while continuously improving reliability. Therefore, how to effectively cope with jamming becomes significantly important to the GNSS receivers.

Because the satellite is far from the ground, the power of the satellite signal is very weak when it reaches the front end of the receiver. RFI is a greatly harmful jamming pattern for GNSS receivers. The existence of RFI will make the working condition of the receiver worse, which leads to the performance of receiver degradation or even positioning failure [5].

The common methods of GNSS interference suppression include the automatic gain control (AGC) method, time-domain method, and frequency domain method. The AGC method is suitable for suppressing strong interference by controlling the gain in the front-end of the receiver [6] [7]. However, the effectiveness of the AGC method decreases in a weak jamming environment. Time-domain interference is predictable mainly based on the difference between the expected signal and the interference signal. But the time-domain method has a poor suppression effect on wideband interference with thermal noise [8] [9]. In the frequency domain, the interference can be suppressed according to the difference in the spectrum line between the signal and the interference. The ability of the frequency domain method will decrease, while the interference is a non-stationary signal [10] [11].

All of these methods have limitations. Time-frequency (TF) analysis has become a major research focus in the field of signal processing, especially for non-stationary signal processing [12] [13] [14] [15]. Short-Time Fourier Transform (STFT) is based on Fourier transform (FT) plus window function to analyze non-stationary signals. The time-frequency analysis capability of STFT is affected by window function [15] [16] [17]. Wigner-Ville Distribution (WVD) does not require a time-frequency window, so aggregation can be obtained good TF distribution image. WVD is very suitable for single component linear frequency modulation interference processing. But the limitation of WVD is that there is crossover in multi-component interference detection [12] [13] [18].

The FrFT is derived from the FT by introducing a linear operator to the one-dimensional Fourier transform. The signal is mapped to a two-dimensional time-frequency plane, which can be rotated at any angle and fully reflect the signal over time-frequency distribution characteristics of changes [19]. Compared with the former two methods, FrFT is a time-frequency analysis method with unique advantages in swept-frequency interference detection [20]. It can not only be understood as a chirp basis decomposition, but also has no cross-interference problem. The energy concentration of the chirp signal will change with the order in the FrFT domain. FrFT transforms the Chirp signal interference detection and separation problem into an optimal order problem [21]. The signal will form an energy peak after the optimal order FrFT, and interference suppression can be realized by processing under the threshold in FrFT domain.

To sum up, the traditional time-frequency analysis method can not detect and suppress the interference signal effectively. In this paper, the proposed method is verified experimentally by a real GPS L1 C/A signal and the interference generated by jammers. Furthermore, the threshold setting of the fractional-order domain is studied systematically. The analysis results show that this method can eliminate the sweep interference accurately.

2. GNSS Signal and Interference Model

The signal received by the GNSS receiver in the presence of radio frequency interference can be written as [12] [15] [18]:

$$y_{RF}(t)=\sum_{i=1}^{N_S} r_i(t)+j(t)+\eta(t) \tag{1}$$

where $r_i(t)$ represents the i^{th} GNSS signal ($i=1,2,\cdots,N_s$), N_s denotes the number of satellites in view, and $j(t)$ is the disturbing term, which the specific expression is determined by the type of interference signal, $\eta(t)$ represents additive white Gaussian noise (AWGN) with a mean value of 0. Depending on the satellite navigation system, the received is different. Assuming that the delay from the signal transmitted by the i^{th} satellite to the receiver receiving is τ_i, the space signal (SIS) transmitted by the i^{th} satellite can be written as [12] [15] [18]:

$$r_{RF,i}(t)=A_i c_i(t-\tau_i)d_i(t-\tau_i)\cos\left[2\pi\left(f_{RF}+f_{d,i}\right)t+\varphi_{RF,i}\right] \tag{2}$$

where:

A_i is the amplitude of the i^{th} useful GNSS satellite signal;

τ_i is the propagation delay for the i^{th} satellite signal;

$c_i(t-\tau_i)$ denotes the Pseudo Random Noise (PRN) code sequences, assumed to be the set {−1, 1};

$d_i(t-\tau_i)$ represents the navigation data message;

f_{RF} denotes the carrier center frequency of the GNSS signal. When considering GPS L1 signal, $f_{RF}=f_{L1}=1575.42\text{ MHz}$;

$f_{d,i}$ denotes the Doppler frequency shift affecting the ith useful GNSS signal;

$\varphi_{RF,i}$ is the initial carrier phase offset for the i^{th} useful GNSS signals.

Sweep frequency interference is a non-stationary narrowband continuous wave interference. This article studies the chirp signal in swept-frequency interference, also called linear frequency modulation (LFM), which refers to the linear transformation of the instantaneous frequency with time, which can be expressed as [12] [15] [18]:

$$j(t)=\sqrt{2J}\,\mathrm{e}^{j2\pi\left(f_0 t+\frac{1}{2}kt^2\right)} \tag{3}$$

where:

$\sqrt{2J}$ represents the power of the sweep interference;

f_0 denotes the initial frequency of the sweep interference;

k is the frequency modulation of the sweep interference;

Figure 1 respectively shows the time-domain waveform and spectrum of a sweep interference.

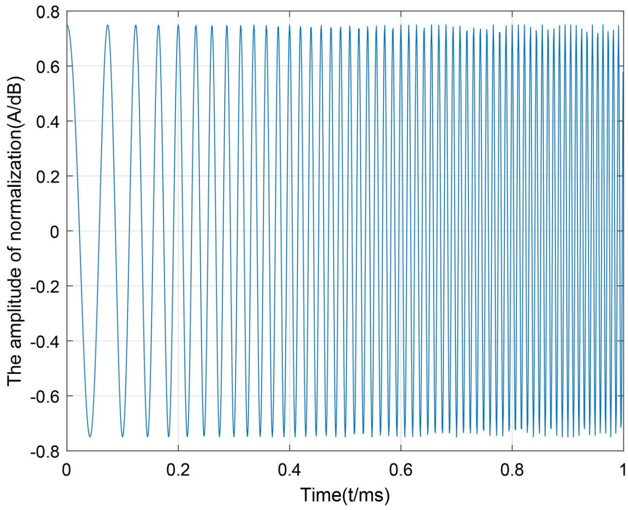

(a)

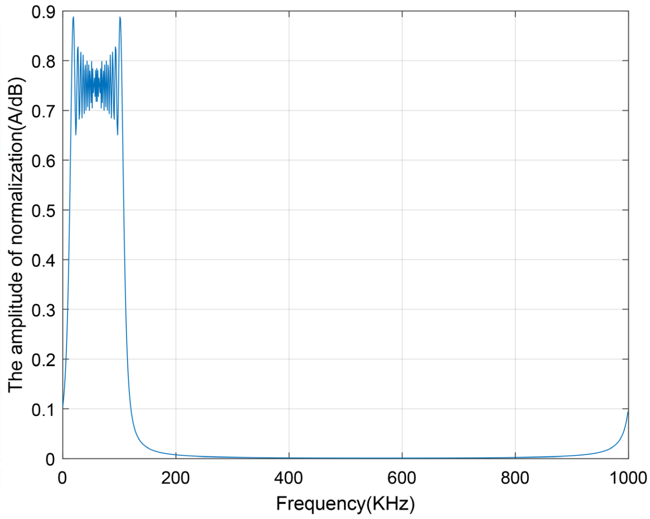

(b)

Figure 1. Interference signal. (a) Chirp waveform; (b) Chirp spectrum.

3. Time Frequency

3.1. STFT

STFT is a commonly used TF distribution for analyzing non-stationary time-varying signals. STFT is derived from FT plus the window function. For a given continuous-time signal $f(t)$, STFT can be defined as [12]-[17] [22]:

$$\mathrm{STFT}(t, f) = \int_{-\infty}^{+\infty} f(\tau) g^{*}(\tau - t) \mathrm{e}^{-j2\pi f\tau} \mathrm{d}\tau \tag{4}$$

where the $g(\tau)$ is the window function and τ is called the lag variable.

However, the shape of STFT's window function determines its TF analysis capability. When the window function area is smaller, the STFT time-frequency analysis ability is stronger, and vice versa. The type and length of the window function should be considered in the STFT analysis of sweep interference. The types of window functions include the Blackman window, Hanning window, Hamming window, and Caser window. The selected window function needs the main lobe to be as narrow as possible, the side lobe gain is small and attenuation to be fast, so that the energy is concentrated in the main lobe and spectrum leakage is reduced. **Figure 2** shows the effect of window function on STFT. The length of the window function also needs to be appropriate. As the length increases, the frequency resolution increases, but it is at the cost of computational complexity. **Figure 3** shows the effect of the length of the window function on STFT.

3.2. WVD

WVD belongs to a typical quadratic or bilinear TF representation since the analyzed signal is used twice in the calculation. The WVD can be defined as the Fourier transform of the time-dependent instantaneous auto-correlation function $R(t,\tau)$ of the analyzed signal, given as [12]-[17] [23]:

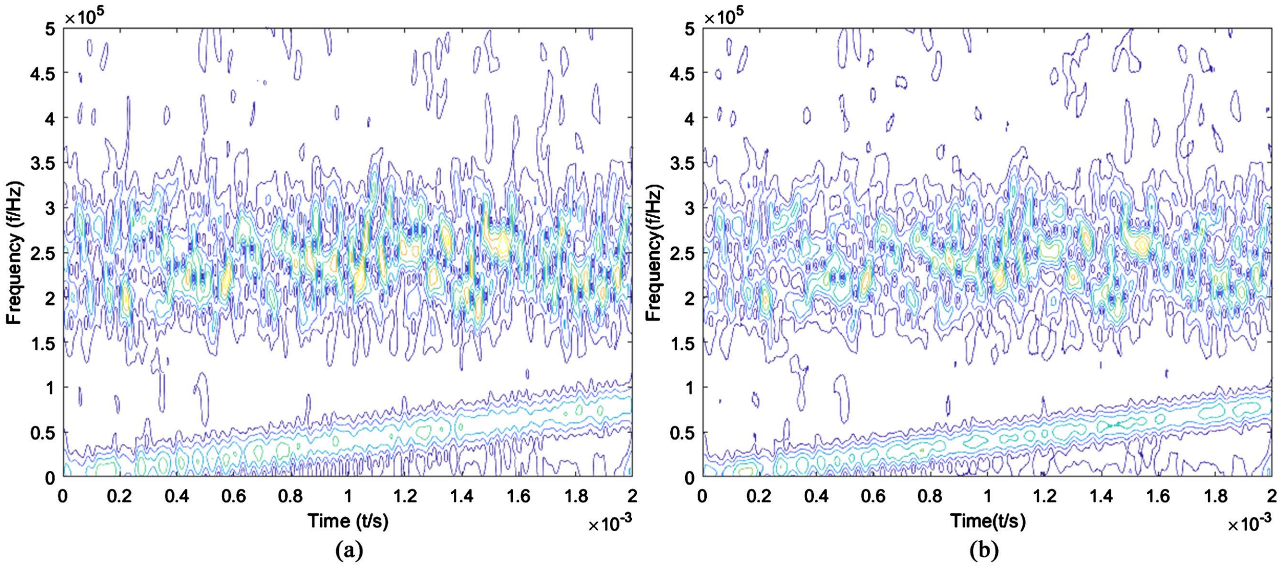

Figure 2. STFT with different windows. (a) Blackman window (N = 63); (b) Hamming window (N = 63).

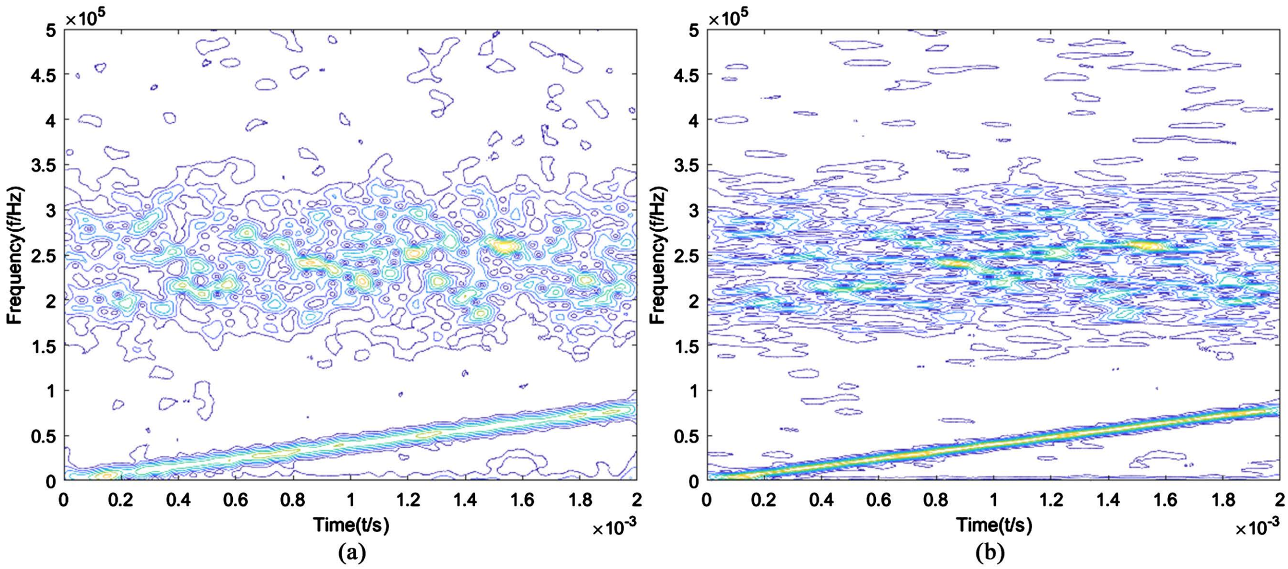

Figure 3. STFT with different lengths of windows. (a) Hamming window (N = 127); (b) Hamming window (N = 255).

$$\mathrm{WVD}(t, f) = \int_{-\infty}^{+\infty} R(t,\tau)\mathrm{e}^{-j2\pi f\tau}\mathrm{d}\tau = \int_{-\infty}^{+\infty} f\left(t+\frac{\tau}{2}\right) f^*\left(t-\frac{\tau}{2}\right)\mathrm{e}^{-jw\tau}\mathrm{d}\tau \tag{5}$$

where, τ is called the lag variable, f is the frequency, the instantaneous correlation function $R(t,\tau)$ is equal to $f\left(t+\frac{\tau}{2}\right) f^*\left(t-\frac{\tau}{2}\right)$.

The time-domain resolution and frequency resolution of the WVD algorithm are better than that of STFT in performance. However, when processing multi-component signals, the calculation results not only contain autocorrelation terms, but also have cross-correlation terms, also known as cross-terms, resulting a decrease in interference detection rate.

Suppose the signal form is as follows:

$$f(t) = f_1(t) + f_2(t) \tag{6}$$

According to the definition of WVD, we can obtain:

$$\mathrm{WVD}_f(t, f) = \mathrm{WVD}_{f_1}(t, f) + \mathrm{WVD}_{f_2}(t, f) + 2Re\{\mathrm{WVD}_{f1,f2}(t, f)\} \tag{7}$$

where the $2Re\{\mathrm{WVD}_{f1,f2}(t, f)\}$ is the cross term, misleading results in the TF analysis. Figure 4 shows the interference detection of WVD.

3.3. FrFT

The algorithm first realizes the detection of sweeping interference through the fractional Fourier transform, then set the threshold to filter the interference. At last, the inverse fractional Fourier transform is used to restore the signal. The p order fractional Fourier transform can be expressed as [19] [20] [21]:

$$F_p(u) = F^p[f(t)](u) = \int_{-\infty}^{+\infty} f(t) K_p(u,t)\,\mathrm{d}t \tag{8}$$

$$K_P(u,t) = \begin{cases} A_a \exp\left[j\pi\left(u^2\cot\alpha - 2ut\csc\alpha + t^2\cot a\right)\right], \alpha \neq n\pi \\ \delta(t-u), \alpha = 2n\pi \\ \delta(t+u), a = (2n\pm 1)\pi \end{cases} \tag{9}$$

where, $f(t)$ is the analyzed signal; u means the fractional Fourier domain; p is the order of the FrFT; $F^p[\cdot]$ means the FrFT's rotation operator; $K_P(u,t)$ is the Kernel function.

In the kernel function of the fractional Fourier transform, where:

$$A_a = \frac{\exp\left[-\dfrac{j\pi\,\mathrm{sgn}(\sin a)}{4} + ja/2\right]}{|\sin a|^{\frac{1}{2}}}, a = \frac{p\pi}{2} \tag{10}$$

At the same time, the expression of Inverse Fractional Fourier Transform (IFRFT) is:

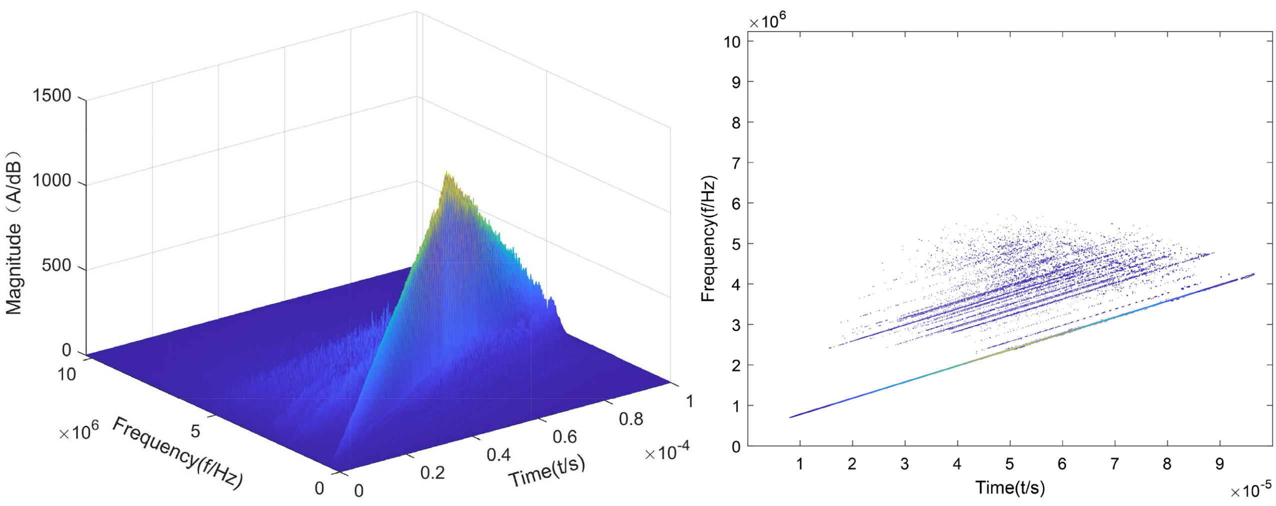

Figure 4. The interference detection of WVD. (a) WVD; (b) The contour of WVD.

$$f(t) = F^{-P}\left[F_P(u)K_P^*(u,t)\mathrm{d}t\right] \tag{11}$$

The FrFT of the signal corresponds to the counterclockwise rotation of the TF plane. When rotated to a suitable angle (optimal order), the signal gathers energy in the TF plane. We can perform the fractional Fourier transform of the signal according to the relationship between the fractional Fourier transform and the time and frequency plane of WVD. The fractional-order Fourier transform of the original signal is perpendicular to the WVD time-frequency plane. **Figure 5** shows the relationship between the FrFT and the TF plane of WVD.

The linear regular matrix transformation of p order FrFT can be defined as follows:

$$M = \begin{bmatrix} A & B \\ C & D \end{bmatrix} = \begin{bmatrix} \cos\alpha & \sin\alpha \\ -\sin\alpha & \cos\alpha \end{bmatrix} \tag{12}$$

This matrix is a two dimensional rotation matrix in the time-frequency plane presents the angle between the p-order fractional Fourier transform of the signal and the frequency plane of WVD. The relation between the p-order and the rotation angle α of the time-frequency plane is as follows:

$$\alpha = \frac{\pi}{2}p \tag{13}$$

In other words, the signal's FrFT of order p corresponds to the clockwise rotation of the signal's WVD at angle α in the time-frequency plane. Its definition is as follows [12] [13]:

$$W_p(u,v) = W_x(u\cos\alpha - v\sin\alpha, u\sin\alpha - v\cos\alpha) \tag{14}$$

where the $W_p(\cdot)$ represents the p-order FrFT of the signal, $W_x(\cdot)$ represents the WVD of the signal. The u and v represent the variables of the rotation system, and the relationship between the rotated coordinates and the original coordinates is:

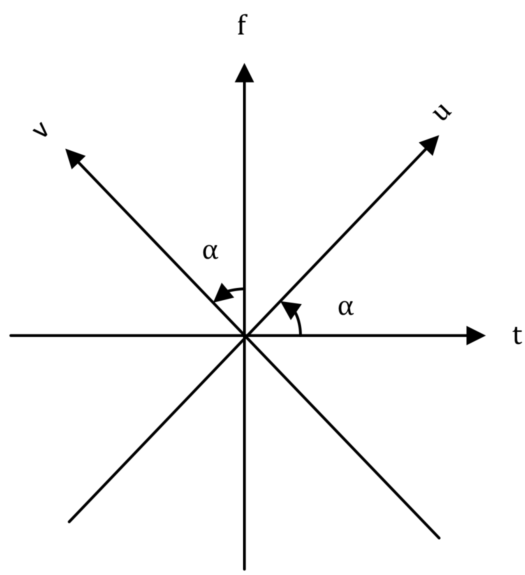

Figure 5. Geometric representation of FrFT.

$$\begin{bmatrix} u \\ v \end{bmatrix} = \begin{bmatrix} \cos\alpha & \sin\alpha \\ -\sin\alpha & \cos\alpha \end{bmatrix} \begin{bmatrix} t \\ f \end{bmatrix} \tag{15}$$

At the same time, the amplitude of GNSS signal is still uniform and flat. According to the above characteristics, interference can be detected by searching the maximum amplitude of fractional Fourier transform of signal.

In this paper, we use the peak search method. The range of rotation angle is [0, 2π], and the value range of the corresponding order is [0, 2], so we can select the step size to calculate the FRFT of the GNSS signal respectively. The peak point corresponding to each rotation order p is recorded, and then compared respectively. When $p = p_0$, corresponding $u = u_0$, the maximum peak point is obtained at this time, which is the corresponding optimal order. Figure 6 shows the interference detection based on FrFT.

After interference detection, we deal with spectral lines in FrFT domain by setting thresholds. The Threshold setting in FrFT domain is an extension of frequency-domain method. The common spectral line resection methods are the fixed method and mean method. 40% of the maximum signal power spectrum is set as the threshold value, which is called the fixed method. The mean method sets the threshold as the average of all spectral line energies. However, neither of these two methods can accurately suppress the interference, causing great damage to the satellite signal. This paper presents a threshold setting method based on detection probability [24].

A satellite signal contains a lot of noise, so it can be modeled as Gaussian noise with zero mean value σ. Since the FrFT is a linear transformation, the transformed signal still obeys the Gaussian distribution. Suppose the probability density function of white noise with zero mean variance σ^2 is $P(x)$, then can be provided as:

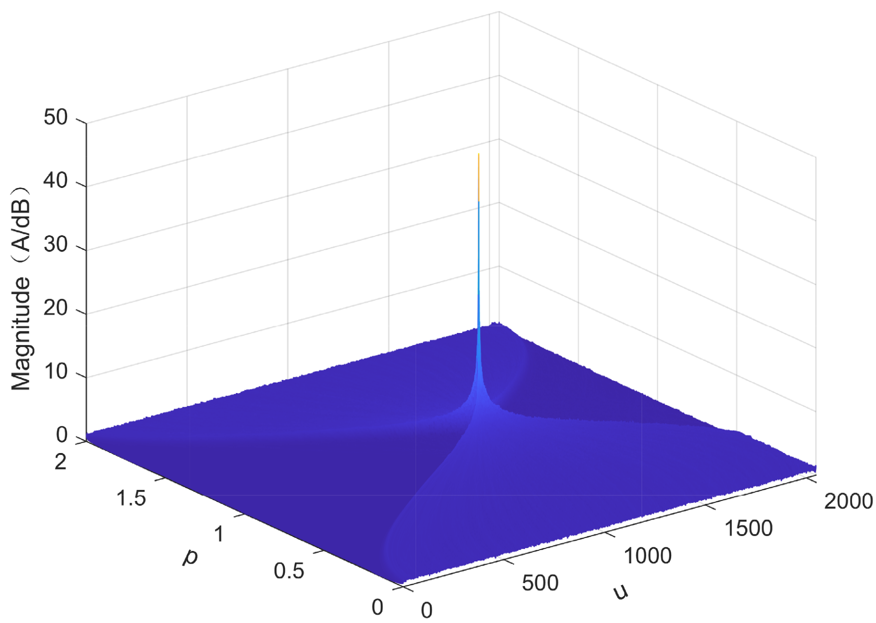

Figure 6. The interference detection of FrFT.

$$P(x)=\frac{1}{\sigma\sqrt{2\pi}}\mathrm{e}^{-\frac{x^2}{2\sigma^2}} \tag{16}$$

If the false alarm probability is P_{fa}, the threshold value is Th, then there is:

$$\begin{aligned} P_{fa} &= 2\int_{Th}^{\infty} P(x) = 2\int_{Th}^{\infty}\frac{1}{\sigma\sqrt{2\pi}}\mathrm{e}^{-\frac{x^2}{2\sigma^2}}\mathrm{d}x \\ &= \frac{2}{\sqrt{\pi}}\int_{\frac{Th}{\sqrt{2}\sigma}}^{\infty}\mathrm{e}^{-t^2}\mathrm{d}t = erfc\left(\frac{Th}{\sqrt{2}\sigma}\right) \end{aligned} \tag{17}$$

According to the above formula, the threshold value is:

$$Th=\sigma\sqrt{2}erfc^{-1}\left(P_{fa}\right) \tag{18}$$

In order to minimize the loss of useful signals, we set the spectral line near u_0 that exceeds the threshold value to zero. Finally, we can get the time domain signal by p fractional inverse transformation of the processed data.

4. Simulation Results and Analysis

In this section, the performance of GNSS interference detection based on FrFT was analyzed in comparison with the traditional TF analysis of STFT and WVD. At the same time, the interference suppression effects based on different thresholds are compared in the simulation. GNSS signal adopts real GPS L1-C/A. And a jammer controlled by a computer was used to produce sweep interference, which was added to the GPS L1-C/A collected by the GNSS software receiver. The experiment parameter for the test is listed in **Table 1**.

In the experiment, the carrier-to-noise power density ratio (C/N_0) of the received GPS L1-C/A signal was 42 dB-Hz, the jamming-to-noise power density ratio (JNR) was 3 dB. The initial frequency f_0 of the linear chirp interference was set to 2.5 MHz, the sweep period of the linear chirp interference was set to 1 ms and the chirp rate k was chosen to be 14 kMHz/s.

This experiment is divided into two parts, including interference detection and interference suppression. In the interference detection part, the signal is processed by the interference detection module. Due to sweep interference being time-varying interference, the time-domain method cannot filter the sweep

Table 1. The experimental setting parameters in the GNSS anti-interference.

Parameter	Value
Carrier-to-noise power density ratio, C/N_0	42 dB-Hz
Jamming-to-noise power density ratio, JNR	2 dB
Sampling frequency, f_s	20 MHz
Intermediate frequency, f_{IF}	4 MHz
Sweep interference initial frequency, f_0	2.5 MHz
Sweep interference sweep period, t_j	1 ms
Sweep interference chirp rate, k	14 kMHz/s

interference from satellite signals. **Figure 7** represents the time domain waveform of the GPS signal interfered with by the sweep signal. It also shows that it is difficult to separate the interference from the useful signal in the time domain.

The sweep signal has a good aggregation effect in the fractional domain, and the distribution of the GNSS spread spectrum signal in the fractional domain is similar to the noise distribution. In this experiment, the iterative method is used to solve the optimal order. **Figure 8** shows the three-dimensional energy aggregation in the FrFT domain and the projection in u domain of the GPS L1-C/A signal

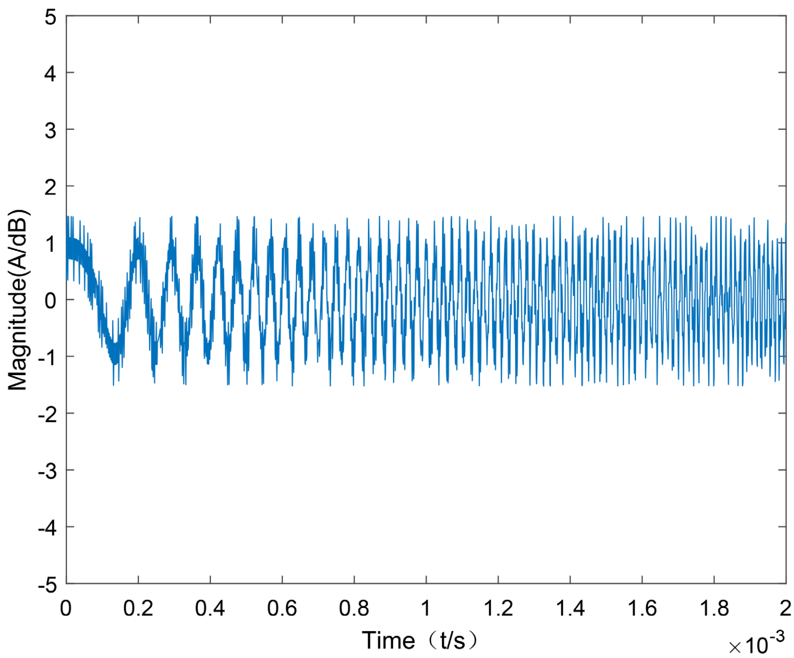

Figure 7. GPS signal disturbed by sweep frequency.

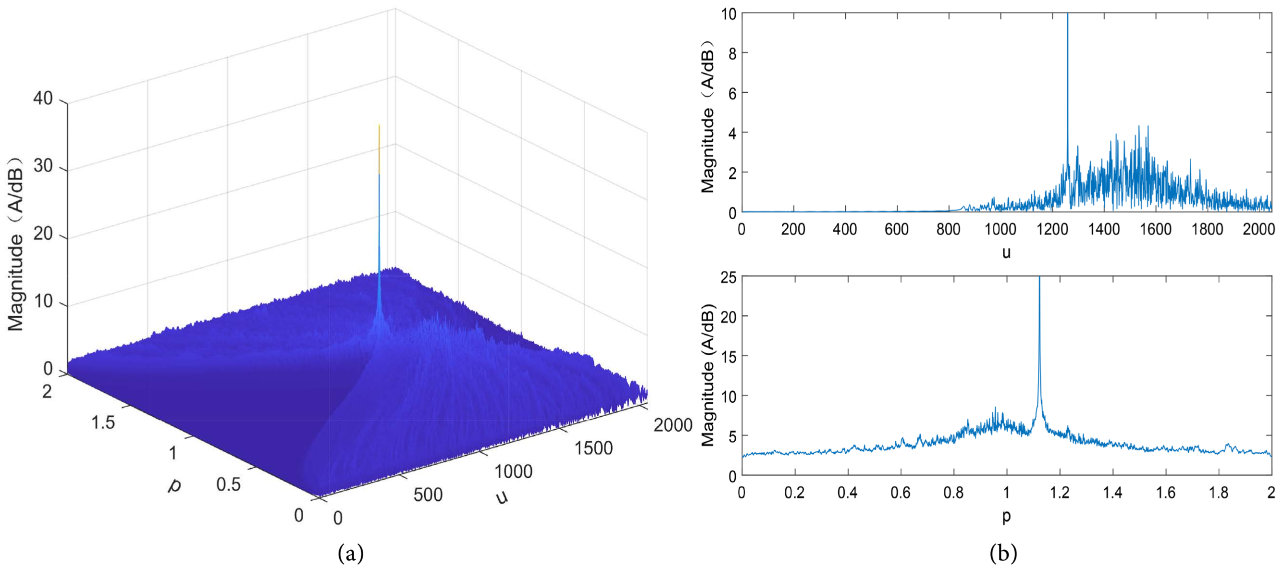

Figure 8. The interference signal is represented in the fractional order domain. (a) The FrFT of the GPS L1-C/A signal in the presence of sweep interference; (b) u in the FrFT domain.

disturbed by frequency sweep.

Figure 8 represents the modulus of GPS L1 signal disturbed by sweep frequency under the optimal FrFT distribution. Figure 8(a) shows that the sweep interference concentrates at the energy peak after FrFT. The maximum peak point means that the optimal $p_0 = 1.012$, $u_0 = 1125$. Figure 8(b) shows the rotation of the time-frequency plane into u domain. Interference detection can be achieved according to the position of the spectrum peak in Figure 8.

The estimation RMSE of initial frequency and modulated frequency by different methods is compared. The smaller the error, the better the detection effect, while the JNR is a certain value. The mean square error of initial frequency and modulated frequency based on FrFT is minimum, and the detection performance is improved by about one order of magnitude. Figure 9 shows the interference detection effect under different simultaneous frequency analysis methods.

In Figure 9, the RMSE level of the GNSS sweep interference initial frequency estimate with the STFT and the WVD is all above of 10^{-2} level, while the RMSE level of the GNSS sweep interference modulation frequency estimate with the STFT and WVD is above of 10^{-3} level.

The RMSE level of the GNSS sweep interference initial frequency estimate based on FrFT was almost kept below 10^{-2} level, and the RMSE level of modulation frequency rate keep below 10^{-5} level. The smaller the error, the better the detection effect, while the JNR is a certain value. The mean square error of initial frequency and modulated frequency based on FrFT is minimum, and the detection performance is improved by about a least one order of magnitude.

In the interference suppression part, the effectiveness of the detection probability threshold method is verified at first. If the signal can be captured by the receiver after interference suppression, it shows the effectiveness of the algorithm.

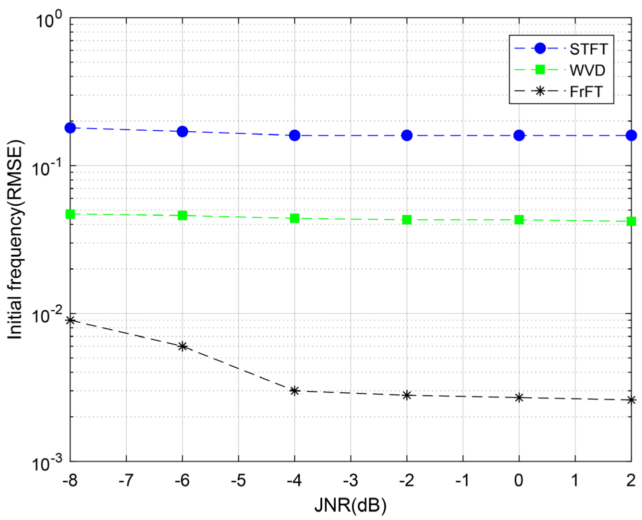

(a)

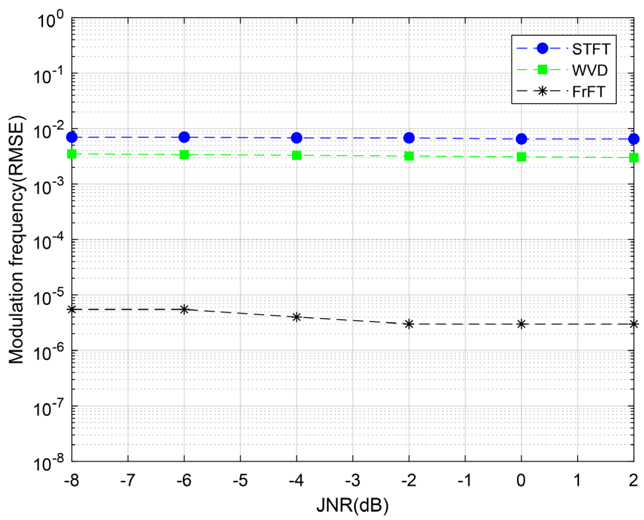

(b)

Figure 9. The disturbed signal is detected by using STFT, WVD, and FrFT, respectively. The RMSE of the estimated modulated frequency rate and initial frequency of the sweep interference is presented. (a) The estimation RMSE of initial frequency; (b) The estimation RMSE of modulated frequency.

This acquisition experiment uses 60 ms GPS data to simulate the proposed method. The carrier frequency is 4 Mhz, the sampling rate is 20 Mhz. The detection probability P_{fa} was set to 0.001 in the experiment. The threshold value of this experiment can be obtained according to the Formula (18). The correlation between the local carrier and the GPS L1-CA jammed after suppression is used to judge the effectiveness of the interference suppression method.

Satellite signals contain coded delay information and doppler frequency shift information. The GNSS receiver gets the user's position, speed, and time by demodulation of the satellite signals. The code phase and Doppler shift information can be obtained when the local carrier is completely related to the received information. Figure 10(a) shows the GPS-L1 C/A signal can not be used by receivers. Figure 10(b) shows a clear peak, which means that the coded delay bins and the doppler frequency bins can be obtained in the signal from the RF front end of a receiver. This also proves the effectiveness of the FrFT interference suppression method based on the detection probability threshold.

The better the interference suppression algorithm is, the higher the SNR of the system is. Therefore, SNR can be defined to compare the effect of interference suppression under different thresholds. The SNR can be expressed as:

$$\mathrm{SNR} = 10\lg\left\{\frac{\sum s^2(t)}{\sum\left(s(t)-\hat{s}(t)\right)^2}\right\} \tag{19}$$

Figure 11 shows the SNR under the fixed method and mean method and the proposed method.

As can be seen from Figure 11, the interference in the satellite signal becomes more and more serious with the increase of JNR. If there is no interference suppression measure, the value of a_{mean} will drop rapidly and reach the lowest value,

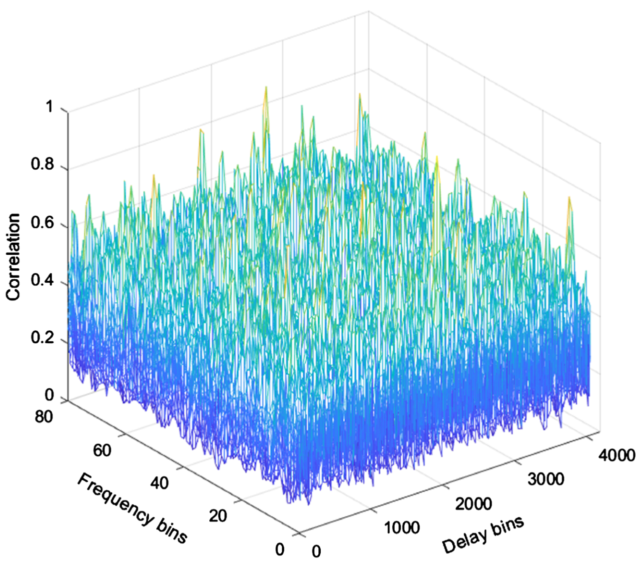

(a)

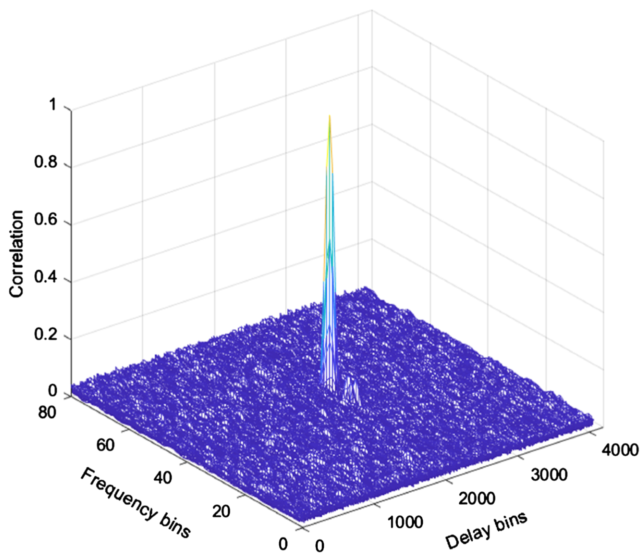

(b)

Figure 10. The result of capturing by the proposed threshold method. (a) No interference suppression; (b) The interference suppression of proposed method.

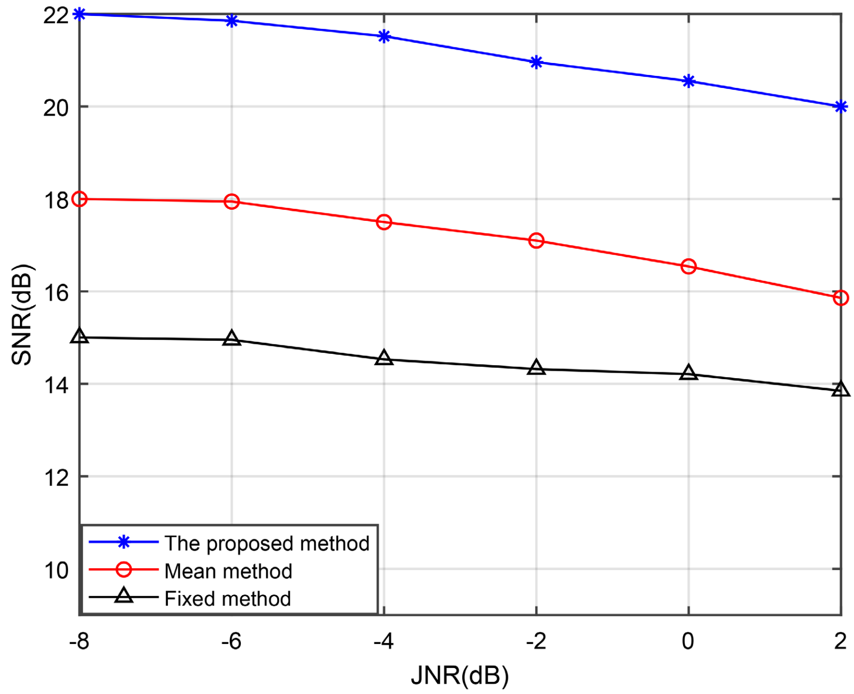

Figure 11. Interference suppression effect under different threshold in FrFT domain.

and the acquisition performance is poor or even cannot be captured. When the SNR is lower than 15dB, the signal is completely distorted and cannot be used. When JNR = 2 dB, the threshold method based on detection probability is still effective, and the interference tolerance is increased by 5 dB compared with the mean threshold method, and by 8 dB compared with the fixed threshold.

5. Conclusion

This paper mainly studies the time-frequency analysis to suppress interference. Through real experimental results, the correctness of the interference detection and suppression method in the FrFT domain is verified. Experiments are performed on the GPS L1-C/A signal in the presence of sweep interference. In the aspect of interference detection, the method based on fractional-order Fourier transform is better than the conventional STFT and WVD detection. The RMSE level of the GNSS sweep interference initial frequency estimate with the STFT and the WVD is all above of 10^{-2} level, while the RMSE level of the GNSS sweep interference modulation frequency estimate with the STFT and WVD is above of 10^{-3} level. In the aspect of interference suppression, the threshold method based on detection probability proposed in this paper has a better interference suppression effect than conventional methods such as fixed threshold and mean threshold. At the same time, the interference tolerance is improved by the proposed method. Because the intensity of interference will change with the environment, how to set the adaptive threshold will be the direction of improving the performance of interference suppression in the fractional-order domain.

Conflicts of Interest

The author declares no conflicts of interest regarding the publication of this paper.

References

[1] Fernandez-Prades, C., Presti, L.L. and Falletti, E. (2011) Satellite Radio Localization from GPS to GNSS and Beyond: Novel Technologies and Applications for Civil Mass Market. *Proceedings of the IEEE*, **99**, 1882-1904. https://doi.org/10.1109/JPROC.2011.2158032

[2] Rokaha, B., Gautam, B.P. and Kitani, T. (2019) Building a Reliable and Cost-Effective RTK-GNSS Infrastructure for Precise Positioning of IoT Applications. 2019 *Twelfth International Conference on Mobile Computing and Ubiquitous Network* (*ICMU*), Kathmandu, 4-6 November 2019, 1-4. https://doi.org/10.23919/ICMU48249.2019.9006632

[3] Ioannides, R.T., Pany, T. and Gibbons, G. (2016) Known Vulnerabilities of Global Navigation Satellite Systems, Status, and Potential Mitigation Techniques. *Proceedings of the IEEE*, **104**, 1174-1194. https://doi.org/10.1109/JPROC.2016.2535898

[4] Issam, S.M., Adnane, A. and Madiabdessalam, A. (2020) Anti-Jamming Techniques for Aviation GNSS-Based Navigation Systems: Survey. 2020 *IEEE* 2*nd International Conference on Electronics*, *Control*, *Optimization and Computer Science* (*ICECOCS*), Kenitra, 2-3 December 2020, 1-4. https://doi.org/10.1109/ICECOCS50124.2020.9314449

[5] Wang, P. and Morton, Y.T. (2020) Efficient Weighted Centroid Technique for Crowdsourcing GNSS RFI Localization Using Differential RSS. *IEEE Transactions on Aerospace and Electronic Systems*, **56**, 2471-2477. https://doi.org/10.1109/TAES.2019.2917577

[6] Amoroso, F. (1983) Adaptive A/D Converter to Suppress CW Interference in DSPN Spread-Spectrum Communications. *IEEE Transaction*, **31**, 1117-1123. https://doi.org/10.1109/TCOM.1983.1095753

[7] Bastide, F., Akos, D., Macabiau, C. and Roturier, B. (2003) Automatic Gain Control (AGC) as an Interference Assessment Tool. *Proceedings of the* 16*th International Technical Meeting of the Satellite Division of the Institute of Navigation*, Portland, OR, 9-12 September 2003.

[8] Gao, G.X., De Lorenzo, D.S., Walter, T. and Enge, P. (2007) Acquisition and Tracking of GIOVE-a Broadcast L1/E5/E6 Signals and Analysis of DME/TACAN Interference on Receiver Design. *Proceedings of the European Navigation Conference on Global Navigation Satellite Systems* (*ENC-GNSS* 2007), Geneva, 29 May-1 June 2007.

[9] Palestini, C., Pedone, R., Villanti, M. and Corazza, G.E. (2008) Integrated NAV-COM Systems: Assisted Code Acquisition and Interference Mitigation. *IEEE Systems Journal*, **2**, 48-61. https://doi.org/10.1109/JSYST.2007.914866

[10] Kuriger, G., Grant, H., Cartwright, A. and Heirman, D. (2003) Investigation of Spurious Emissions from Cellular Phones and the Possible Effect on Aircraft Navigation Equipment. *IEEE Transactions on Electromagnetic Compatibility*, **45**, 281-292. https://doi.org/10.1109/TEMC.2003.811309

[11] Raimondi, M., Julien, O., Macabiau, C. and Bastide, F. (2006) Mitigating Pulsed Interference Using Frequency Domain Adaptive Filtering. *Proceedings of the* 19*th International Technical Meeting of the Satellite Division of The Institute of Navigation* (*ION GNSS* 2006), Fort Worth, TX, 26-29 September 2006, 2251-2260.

[12] Sun, K., Zhang, M. and Yang, D. (2016) A New Interference Detection Method Based on Joint Hybrid Time-Frequency Distribution for GNSS Receivers. *IEEE Transactions on Vehicular Technology*, **65**, 9057-9071. https://doi.org/10.1109/TVT.2016.2515718

[13] Borio, D., Camoriano, L., Savasta, S. and Presti, L.L. (2008) Time-Frequency Excision for GNSS Applications. *IEEE Systems Journal*, **2**, 27-37. https://doi.org/10.1109/JSYST.2007.914914

[14] Motella, B., Savasta, S., Margaria, D. and Dovis, F. (2008) Method for Assessing the Interference Impact on GNSS Receivers. *IEEE Transactions on Aerospace and Electronic Systems*, **47**, 1416-1432. https://doi.org/10.1109/TAES.2011.5751267

[15] Sun, K., Liu, W., Xu, H. and Yang, D. (2013) Interference Detection Based on Time-Frequency Analysis for GNSS. *Proceedings of the* 26*th International Technical Meeting of the Satellite Division of the Institute of Navigation*, Nashville, 16-20 September 2013.

[16] Silvius, M., Lindsey, A.R. and Hughes, D.H. (2013) Broadband Interference Mitigator for Global Positioning System Using Time-Frequency Domain Excision Filtering. *Proceedings of SPIE—The International Society for Optical Engineering*, **15**, 14-17. https://doi.org/10.1117/12.506102

[17] Rezaei, M.J., Abedi, M. and Mosavi, M.R. (2016) New GPS Anti-Jamming System Based on Multiple Short-Time Fourier Transform. *IET Radar Sonar & Navigation*, **10**, 807-815. https://doi.org/10.1049/iet-rsn.2015.0417

[18] Sun, K. (2021) A New GNSS Interference Detection Method Based on Rearranged Wavelet-Hough Transform. *Sensors*, **21**, Article 1714. https://doi.org/10.3390/s21051714

[19] Almeida, L.B. (1994) The Fractional Fourier Transform and Time-Frequency Representations. *IEEE Transactions on Signal Processing*, **42**, 3084-3091. https://doi.org/10.1109/78.330368

[20] Bo, X.A., Xl, A. and Cwa, B. (2021) Estimation of Chirp Signals Based on Fractional Fourier Transform Combined with Otsu's Method. *Optik*, **240**, Article ID: 166945.

[21] Ozaktas, H.M., Arikan, O., Kutay, M.A. and Bozdagt, G. (1996) Digital Computation of the Fractional Fourier Transform. *IEEE Transactions on Signal Processing*, **44**, 2141-2150. https://doi.org/10.1109/78.536672

[22] Ouyang, X. and Amin, M.G. (2001) Short-Time Fourier Transform Receiver for Non-Stationary Interference Excision in Direct Sequence Spread Spectrum Communications. *IEEE Transactions on Signal Processing*, **49**, 851-863. https://doi.org/10.1109/78.912929

[23] Boashash, B. and Black, P.J. (1987) An Efficient Real-Time Implementation of the Wigner-Ville Distribution. *IEEE Transactions on Acoustics, Speech, and Signal Processing*, **35**, 1611-1618. https://doi.org/10.1109/TASSP.1987.1165070

[24] Wang, P., Cetin, E., Dempster, A.G., *et al.* (2017) GNSS Interference Detection Using Statistical Analysis in the Time-Frequency Domain. *IEEE Transactions on Aerospace and Electronic Systems*, **54**, 416-428. https://doi.org/10.1109/TAES.2017.2760658